Control of Nanostructure in Mixtures of Block Copolymers: Curvature Control via Cosurfactant Effects

Feng Chen,[†] Yoshiro Kondo,[†,§] and Takeji Hashimoto*[,†,‡,⊥]

Department of Polymer Chemistry, Graduate School of Engineering, Kyoto University, Katsura, Kyoto 615-8510, Japan, and Advanced Science Research Center (ASRC), Japan Atomic Energy Agency (JAEA), Tokai-Mura, Naka-gun, Ibaraki 319-1195, Japan

Received February 2, 2007; Revised Manuscript Received March 7, 2007

ABSTRACT: We aim to elucidate the cosurfactant effects, which are expected when junctions of two block copolymers share a common microdomain interface, on morphology and phase behavior of mixtures. Especially this paper addresses the effects involved for binary mixtures composed of polystyrene-*block*-polyisoprene having about equal molecular weights but complementary compositions, one forming polystyrene (PS) cylinders in polyisoprene (PI) matrix and the other forming PI cylinders in PS matrix. Transmission electron microscopy and small-angle X-ray scattering were used to characterize the phase behavior and domain spacing of the binary mixtures. First, we found an expanding composition range for hexagonally packed cylindrical morphology and a narrowed composition range for lamellae relative to the corresponding composition ranges for neat SI block copolymer under a strong segregation condition. The result indicates that the cosurfactant effects help a block copolymer to take its spontaneous curvature. Second, it was found that the effects enlarged the domain size and interdomain distance of the binary mixtures. Those results were compared with the theory by Birshtein and co-workers, which is proposed to describe the microdomain morphology for strongly segregated binary block copolymers. We found good agreements between experimental and theoretical results in terms of (i) domain size, (ii) interdomain distance, and (iii) the blending compositions where morphological transitions occur.

I. Introduction

It is well know that block copolymers (bcps) show various kinds of microdomain structures having nanoperiodicity depending on volume fraction of one component block. It is also well-known that a short bcp forms a small domain and a long bcp forms a large domain. When the long bcp and short bcp mix with each other in the same domain with their chemical junctions on the common interfaces, the long-range interactions between the short chain and the long chain must compete with each other to form the domain.[1−3] How does this competition affect the morphology and size of the nanodomain? In this paper we aim to explore the cosurfactant effects, which are expected when the junctions of two bcps share a common microdomain interface, on morphology and phase behavior of bcp mixtures. Especially in this paper we focus on clarification of the effects for binary mixtures composed of polystyrene-*block*-polyisoprene (PS-*b*-PI) having about equal molecular weights but complementary compositions, one forming polystyrene (PS) cylinders in polyisoprene (PI) matrix and the other forming PI cylinders in PS matrix.

Let us consider a system composed of two immiscible homopolymers A and B, as shown in Figure 1a. The Flory−Huggins segmental interaction parameter between A and B, which depends on competing van der Waals short-range interactions of A−A, B−B, and A−B segments, is assumed to be positive so that the system separates into two macroscopic phases of almost pure A and pure B with a single interface in thermal equilibrium (Figure 1a). The important physical factor in this blend system is competing short-range interactions of A−A, B−B, and A−B segments. On the other hand, with incorporation of a single covalent bond between chain ends of A and B polymers to create diblock copolymers (dibcps), A−B dibcps can achieve microphase separation in which the bulk bcp is nothing other than the assembly of interfaces separating A and B microdomains (Figure 1b). It is very important to realize here that the short-range interactions inherent in the blend interplay with the long-range interactions of A and B. These long-range interactions involve conformational entropy of block chains under the incompressibility requirement inherent in liquids, which is important and inherent in polymer science. The interplay of these two interactions is a key physical factor in bcps and yield long-range-ordered domain structures with various spatial symmetries.[4,5]

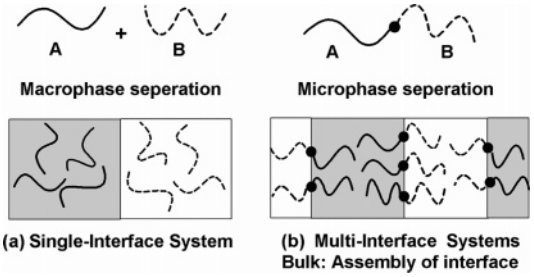

Figure 1. Effects of the connectivity between polymer A and B at their chain ends on the morphology: (a) macrophase separation in the mixtures of homopolymer A and B; (b) microphase separation in A-*b*-B dibcps.

Now we turn to discuss the self-assembly of mixtures of bcps. We have the same short-range interactions between A and B as in neat A−B bcps. However, the long-range interactions of the two bcps (designated hereafter as α and β) themselves now have to compete with each other, which should give new "delicate effects" on nanosized patterns. The competing long-range interactions of α and β will give two cases as schematically

[†] Kyoto University.
[‡] Japan Atomic Energy Agency.
[§] Present address: Tsukuba Research Laboratories, Kuraray Co., Ltd., 41, Miyukigaoka, Tsukuba, Ibaraki 305-0841, Japan.
[⊥] Present address: ASRC, JAEA.

10.1021/ma070297m CCC: $37.00
Published on Web 04/14/2007

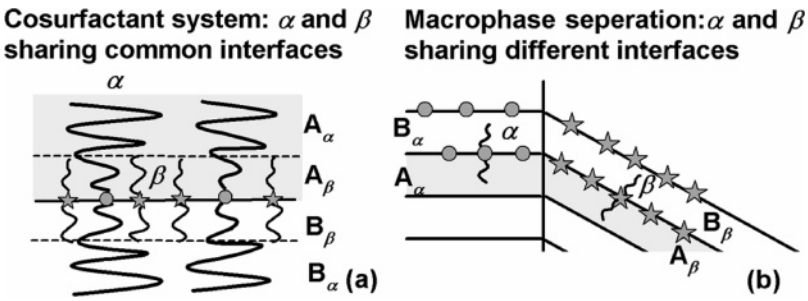

Figure 2. Effects of competing long-range interaction of two A-*b*-B bcps on the morphology of the mixtures of bcps α and *β*, giving rise to cosurfactant effects (part a) and macrophase separation (part b).

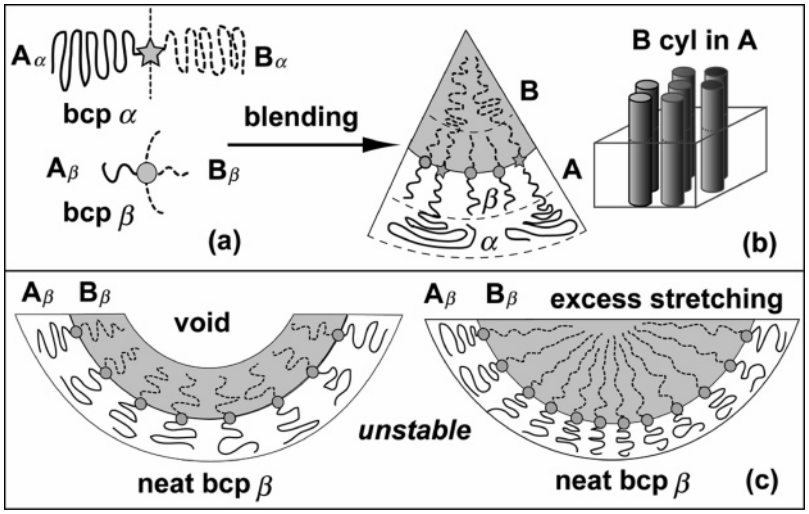

Figure 3. Case of a cosurfactant effect giving rise to an increased interface curvature: (a) packing constraint to satisfy the demand of incompressibility does not allow for a slightly asymmetric bcp *β* to take a spontaneous curvature as shown in part (c), while mixing of a small amout of symmetric long block chains α can release the packing constraint, resulting in formation of cylinder (b).

shown in Figure 2, one in which the two blocks α and *β* are miscible and share common interfaces and act as cosurfactants (part a) and the other in which they are not miscible and share different interfaces (part b), giving rise to macrophase separation in two different ordered phases α and *β*.[6] In this paper, we shall not discuss the systems which undergo macrophase separation but rather discuss the cosurfactant systems. We would like to highlight that the effects promote the bcps to exhibit microdomains having a spontaneous curvature mediated by an asymmetry in the molecular volumes of PS and PI block chains.

Figure 3 shows the case where the cosurfactant effect increases the interface curvature.[7] A long symmetric bcp α having an equal block length for block chain A_α and B_α takes zero spontaneous curvature, giving rise to lamellar morphology, while a slightly asymmetric short bcp *β* having block length of A_β slightly larger than that of B_β takes a small spontaneous curvature (part a). However, many-chain effects on packing the bcp *β* in the domain space do not allow the small spontaneous curvature and end up the flat interface and hence a small lamella. Why is the spontaneous curvature not allowed? The reason is simple: as shown in part c, the packing of many chains with this curvature generates a void in the middle part of the B domains, which is unstable (left-hand side of part c). In order to avoid void formation, the B_β chains must be stretched to fill the space, which causes extra cost of stretching free energy and hence is unstable also (right-hand side of part c). Therefore, the slightly asymmetric short bcp *β* forms a small lamella, instead of cylinder, for example. However, when a small fraction of the large symmetric bcp α is added to the slightly asymmetric short bcp *β*, the large symmetric bcp α will fill the void space and hence will promote the short asymmetric bcp *β* to take its spontaneous curvature (part b).

In another case, the cosurfactant effects tend to decrease interface curvature as schematically shown in Figure 4. A long asymmetric block chain α can form spherical microdomains in bcc lattice (part a). We found out that blending a small amount of a short symmetric bcp *β* effectively changes morphology from bcc spheres to hex cylinder, double gyroid, and lamellae.[8] If one replaces a small fraction of long asymmetric bcp α by the short symmetric chains *β* without changing the curvature and conformations of bcp α, one would create density dip (void as schematically shown in part b). This situation is unstable, so that the neighboring long asymmetric bcp α change their conformations and filled the density dip (part c). This process involves change of the interface curvature from sphere to cylinder or cylinder to lamella (from part b to part c). This is also a manifestation of a cosurfactant effect.

Since Hadziioannou and Skoulios[9] reported the study on the microdomain structure of the blends of bcps by SAXS and TEM, the phase behaviors of the blends of bcps have received considerable experimental[3,6−8,10−17] and theoretical attention.[18−26] A series of studies on binary mixtures of bcps were published by Hashimoto and co-workers, who started studying lamellae-forming bcp blends.[6,27] They extended their investigations to other morphologies later.[3,8] The domain size of binary mixtures of two symmetric PS-*b*-PI copolymers was also explored by Kane et al.[13] Spontak et al.[11] used blends of PS-*b*-PI copolymer of different compositions but similar molecular weights to vary the morphology by changing the relative amounts of the two copolymers. Sakurai and co-workers[15] found an order−order

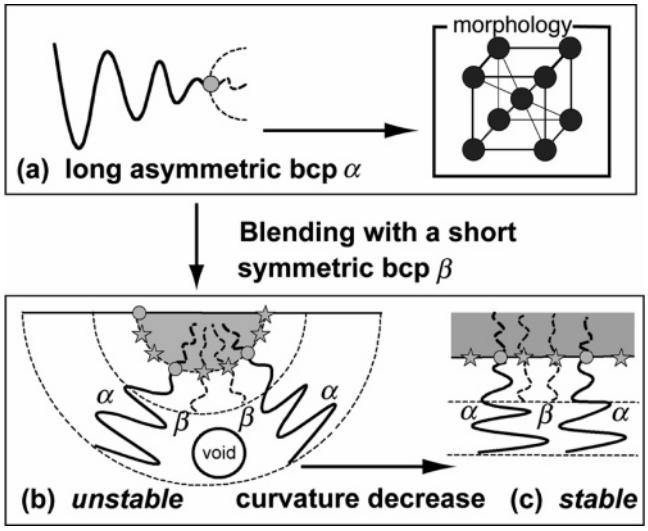

Figure 4. Schematic illustration of a cosurfactant effect which gives rise to a decreasing interface curvature: (a) a long asymmetric bcp α forms bcc spherical domain; (b) a small amount of short symmetrical bcps, which replace the bcp α and which segregate at the interface, leads to regions of low packing density. The creation of density dip destabilizes the spherical morphology. The unstable situation in (b) drives a curvature decrease to enable the long chains α to fill the voids and hence a transition from sphere to cylinder or cylinder to lamella, as shown in the change from part b to part c.

transition between the lamellae and gyroid phase in a mixture of PS-*b*-PI copolymers with increasing temperature.

On the theoretical side, Shi and Noolandi[18,19] predicted the cosurfactant effects using self-consistent-field theory with the strong segregation limit (SSL). They showed that a small amount of short bcp chains at interfaces may shift the phase boundaries of the mixture, suggesting that the morphologies of long bcp can be modified by the addition of short block chains. Matsen[20] constructed phase diagrams for the binary mixtures of two lamellae-forming copolymers but with different molecular weight. He predicted that as the ratios of the molecular weight exceed 5, the blends may phase separate into two distinct lamellar phases, which is consistent with the experimental observation,[3] as depicted in Figure 2b.

In this paper, we continue our effort for the elucidation of the cosurfactant effects for the mixtures of two bcps having equal molecular weight but complementary compositions. We aim to explore how the effect changes morphology and phase behaviors. The experimental results were analyzed in the context of the strong segregation theory proposed by Brishtein, Zhulina, and Lyatskaya.[22−26]

II. Experimental Section

II.1. Samples. Two PS-*b*-PI bcps used in this study were synthesized by sequential living anionic polymerization with *sec*-butyllithium as an initiator and cyclohexane as a solvent. For each synthesis a precursor sample was taken before the second-step polymerization of isoprene to determine the molecular weight of the polystyrene block by size exclusion chromatography. Characteristics of these copolymers designated α and β are summarized in Table 1.

II.2. Preparation of Film Specimens. These two bcps α and β were mixed and dissolved in a homogeneous solution with toluene as a solvent. Film specimens having 16 different blending compositions were obtained by a solution-cast method, as shown in Table 2. Film specimens were cast from the toluene solution containing 5 wt % of polymer in total and then dried until a constant weight was attained. The drying process involved two steps: The slow evaporation process of the solvent for 3 weeks at room temperature; further drying at 60 °C under vacuum until constant weights were attained. The film specimens were further annealed in order to achieve a near-equilibrium state at 130 °C for 24 h under a N_2 atmosphere before SAXS measurements at room temperature and TEM observation.

Table 1. Characteristics of Polystyrene-*block*-polyisoprene Used in This Work

code	$M_n \times 10^{-4}$	M_w/M_n	N_{PS} [a]	N_{PI} [b]	f_{PS} [c]
α	5.12	1.02	101	581	0.185
β	3.75	1.02	263	141	0.705

[a] Number-average degree of polymerization (DP) of a polystyrene block chain. [b] Number-average degree of polymerization (DP) of a polyisoprene block chain. [c] Volume fraction of polystyrene in the dibcps.

II.3. Small-Angle X-ray Scattering. The microdomain structures were investigated by small-angle X-ray scattering (SAXS) using a rotating anode X-ray generator operated at 40 kV and 300 mA. The X-ray monochromated by a graphite crystal has wavelength $\lambda = 0.154$ nm (Cu Kα). The scattered intensity is measured with a one-dimensional position-sensitive proportional counter. SAXS profiles were recorded at room temperature over a period of 30 min and corrected for air scattering, absorption, and thermal diffuse scattering.

II.4. Transmission Electron Microscopy. For transmission electron microscopy (TEM), the film specimens were microtomed at −100 °C, using a Reichert Ultracut E low-temperature sectioning system. The ultrathin sections were stained with the vapor of 2% osmium tetraoxide (OsO_4) solution for a few hours. The stained sections were observed with a JEOL JEM2000FXZ TEM operated at 120 kV. On the TEM images the PI microdomains appear dark, while the PS microdomains appear bright due to the selective staining of PI domains with OsO_4.

III. Results

III.1. Characterization of the Morphology of the Neat Diblock Copolymers. Figure 5 shows the TEM micrographs of neat α and neat β. The dark region corresponds to the OsO_4-stained PI phase, and bright one is the unstained PS phase. Those images show clearly that sample α (image a) exhibits the morphology of PS cylinders in PI matrix, while sample β (image b) consists of PI cylinders in PS matrix. Both of them form hexagonally packed cylinders with long-range order.

The morphologies of the neat bcps were further confirmed by SAXS. The SAXS profiles taken at ambient temperature are shown in Figure 6. The profiles are plotted as a function of magnitude of scattering vector, q, defined as

$$q = (4\pi/\lambda)\sin(\theta/2) \quad (1)$$

where λ and θ are the wavelength of the incident X-ray and the scattering angle, respectively. The scattered intensity is plotted on a logarithmic scale in arbitrary units. On both of the profiles, the position of the first-order maximum (q_m) can be easily determined. We marked the positions of the higher-order scattering maxima by an arrow with number. The SAXS profiles of neat α and β clearly show five higher-order scattering peaks at positions of $\sqrt{3}$, $\sqrt{4}$, $\sqrt{7}$, $\sqrt{9}$, and $\sqrt{12}$ relative to the position of the first-order peak, indicating that the morphology of these samples is hexagonally packed cylindrical with reasonable long-range order. These SAXS results seem to be in good agreement with TEM images.

III.2. Morphological Study of Binary Mixtures by TEM. The typical TEM images of six representative mixtures (90/10, 65/35, 60/40, 40/60, 30/70, and 20/80) of samples α and β described in Table 2 are displayed in Figure 7. The 90/10 and 65/35 blends (a and b, respectively) appear to exhibit the PS cylinders in PI matrix, while the 60/40 and 40/60 blends (c and

Table 2. Characteristics of the Blend Specimens Studied in This Paper

	α/β wt %/wt %[a]															
	90/10	83/17	81/19	78/22	75/25	70/30	65/35	60/40	55/45	50/50	40/60	30/70	20/80	15/85	10/90	5/95
ϕ_{PS}[b]	0.24	0.27	0.28	0.30	0.31	0.34	0.36	0.39	0.40	0.43	0.48	0.54	0.60	0.62	0.65	0.67
morphology[c]	PS-cyl	PS-cyl	PS-cyl	PS-cyl	PS-cyl	PS-cyl	PS-cyl	lam	lam	lam	lam	gyroid	PI-cyl	PI-cyl	PI-cyl	PI-cyl
D (nm)[d]	38.8	45.4	48.9	47.6	49.5	47.5	48.8	43.1	42.8	42.2	41.4		43.9	43.4	41.7	40.5
R (nm)[e]	9.98	12.4	13.6	13.6	14.5	14.5	15.4	16.7	17.2	18.1	19.7		14.7	14.0	13.0	12.2

[a] Blend composition. [b] Net volume fraction of PS block chains in blends given by $\phi_{PS} = (g_\alpha w_{PS}^\alpha + g_\beta w_{PS}^\beta)/\{g_\alpha w_{PS}^\alpha + g_\beta w_{PS}^\beta + \rho_{PS}\rho_{PI}^{-1}[g_\alpha(1 - w_{PS}^\alpha) + g_\beta(1 - w_{PS}^\beta)]\}$, where g_α and g_β are the weight fraction of α and β in the blends; w_{PS}^α and w_{PS}^β are the weight fractions of polystyrene blocks in neat α and β; $\rho_{PS} = 1.0514$ g/cm^3 and $\rho_{PI} = 0.925$ g/cm^3. [c] Determined by SAXS and TEM. [d] Interdomain distance. [e] Radius of cylinder as calculated by $R_i = (\sqrt{3}/2\pi)^{0.5}\phi_i^{0.5}D$, where i = PS or PI, or thickness of PS lamella as calculated by $L_{PS} = D\phi_{PS}$.

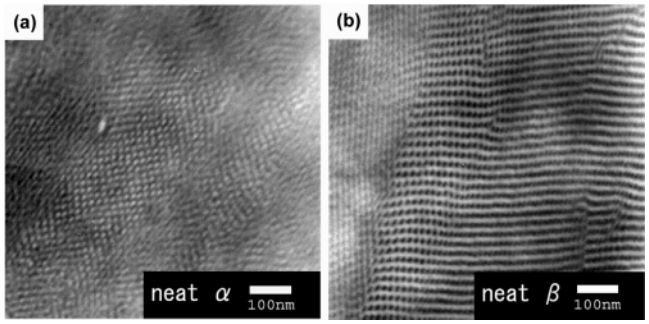

Figure 5. Transmission electron micrographs of samples α and β. Sample α (part a) exhibits the PS cylinders in PI matrix, while sample β (part b) consists of PI cylinders in PS matrix. The PI microdomains appear dark due to selective staining with OsO_4.

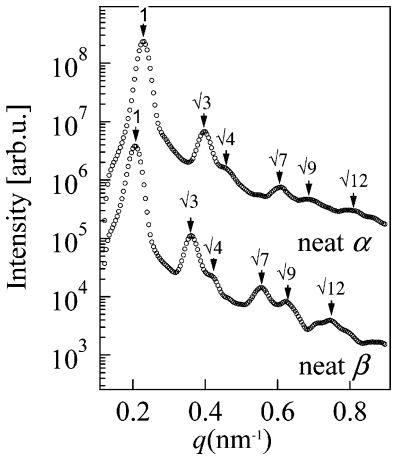

Figure 6. SAXS profiles of neat α and β reveal that the two bcps form hexagonally packed cylindrical morphologies.

d) consist of alternating PS and PI lamellae. The image (e) corresponding to the 30/70 blend shows the uniform and regular "wagon-wheel" pattern, which is consistent with the [111] projection of the gyroid phase, indicating that this blend forms double-gyroid structure of PI in the matrix of PS. We discern that the 20/80 mixture consists of PI cylinders in PS matrix, as shown in Figure 7f. Note that we studied the morphologies of the other blends also as described in Table 2 by TEM, though they are not presented in this paper. Those TEM images show that the other five blends (83/17, 81/19, 78/22, 75/25, and 70/30) with composition in the range between 90/10 and 65/35 form PS cylinders in PI matrix, while the other two mixtures (55/45 and 50/50) with composition between 60/40 and 40/60 possess alternating lamellae structure. When the weight fraction of α in the mixtures (15/85, 10/90, and 5/95) is less than 20%, the blend mixtures form the PI cylinders in a PS matrix.

III.3. Morphological Study of Binary Mixtures by SAXS. The SAXS profiles of the seven blend specimens (including those used to produce Figure 7 and the 5/95 blend described in Table 2) measured at room temperature are shown in Figure 8. The profiles are represented as a function of the reduced magnitude of scattering vector, q/q_m, and the scattered intensity is represented on a logarithmic scale in arbitrary units. On each profile, we marked the positions of the higher-order scattering maxima by an arrow with number. The SAXS patterns for the 90/10 and 65/35 blends exhibit respectively two and three higher-order scattering peaks at positions in the ratio of $1{:}\sqrt{4}{:}\sqrt{7}$ and $1{:}\sqrt{4}{:}\sqrt{7}{:}\sqrt{9}$, indicating that the morphology of these samples is hexagonally packed cylindrical. Note that the second-order peak at $\sqrt{3}$ for hexagonally packed cylindrical morphology is relatively weak for 90/10 or even absent for 65/35.

The SAXS profiles of the 60/40 and 40/60 blends clearly show four higher-order scattering peaks whose positions are integer multiples of the first-order scattering peak position, hence revealing lamellar morphology. With a further increase of the fraction of bcp β in the blend, the SAXS profile dramatically changes; a peak or shoulder appears near the first-order peak. The ratio of peak position can be expressed as $1{:}1.15$ ($1{:}\sqrt{4/3}$), which corresponds to the diffractions from (211) and (220) planes of a double-gyroid phase. Moreover, we can discern a broad peak arising from the third- and fourth-order reflections at position of 2.52 ($\sqrt{19/3}$) and 2.89($\sqrt{25/3}$) overlapping one another, corresponding to the reflections of (532), (611) and (550), (543) planes, respectively. The result indicates that the 30/70 blend exhibits the double-gyroid structure, which is in good agreement with the observation by TEM.

With a further increase of the weight fraction of bcp β in blend, the SAXS profiles (of the blends 20/80 and 5/95) show again a classical powder pattern of hexagonally packed cylindrical morphology lacking the high-order reflection of $\sqrt{3}$ for the 20/80 blend and $\sqrt{4}$ for the 5/95 blend. This result is consistent with our theoretical prediction about the SAXS profile of hexagonally packed cylinders, based on paracrystalline model.[28] The relative intensities of the higher-order maxima at position of $\sqrt{3}$ and $\sqrt{4}$ are sensitive to the composition of the sample. As mention above, we also studied the morphologies of the other blends described in Table 2 by SAXS, though not presented in this paper. Those SAXS profiles show that the other five blends (83/17, 81/19, 78/22, 75/25, and 70/30) with composition in the range between 90/10 and 65/35 form PS cylinders in PI matrix, while the other two mixtures (55/45 and 50/50) with composition between 60/40 and 40/50 possess alternating lamellae structure. When the weight fraction of α in the mixtures (15/85 and 10/90) is less than 20%, the blends form PI cylinders in PS matrix. All SAXS results are consistent with the observation of TEM.

Note that we have investigated SAXS and TEM for the 16 blends. All of them show a single microdomain morphology which depends on blend compositions, implying that α and β are miscible at the molecular level and forming the single microdomain morphologies.

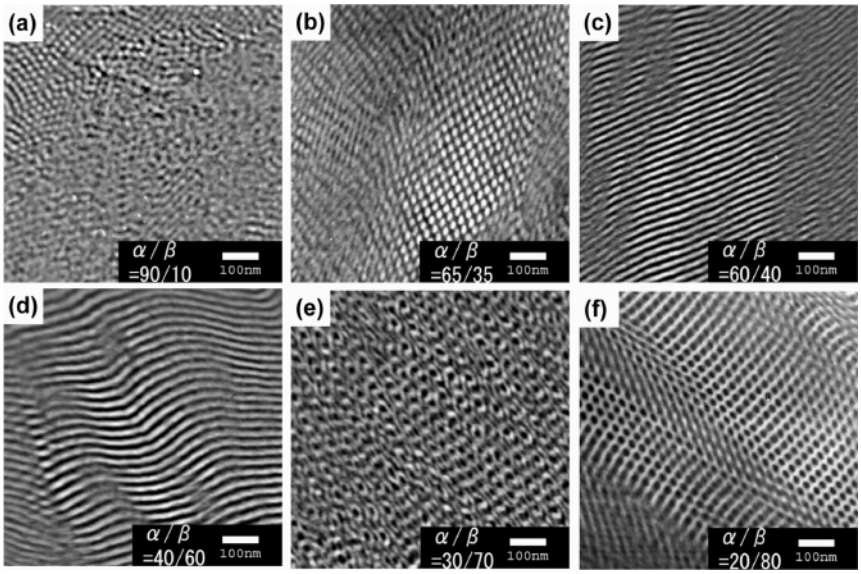

Figure 7. Series of transmission electron micrographs obtained from blends described in Table 2. The 90/10 and 65/35 blends (a and b, respectively) exhibit the PS cylindrical morphology, while the 60/40 and 40/60 blends (c and d) consist of lamellae. The 30/70 blend exhibits a double-gyroid morphology (e), and the 20/80 blend consists of PI cylinders (f).

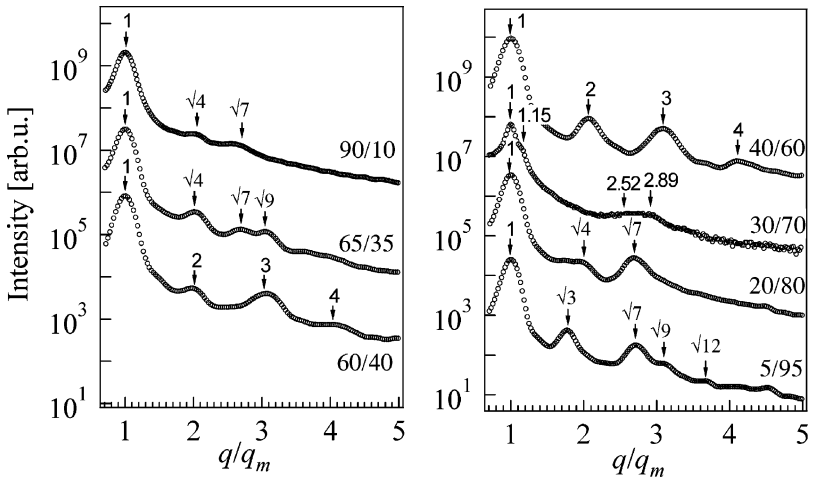

Figure 8. Series of SAXS profiles from blends of α/*β* with different compositions. The 90/10 and 65/35 blends (a and b, respectively) show a typical profile for hex cylinder morphology, while the 60/40 and 40/60 blends (c and d) consist of lamellae. The 30/70 blend exhibits a double-gyroid morphology (e), and the 20/80 and 5/95 blends consists of PI cylinders (f).

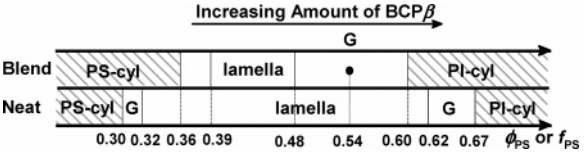

Figure 9. Summary of morphological investigation of the blends of PS-*b*-PI bcps α/*β* with increasing amount of *β* bcp or volume fraction of PS block in the blends in comparison with the result of PS-*b*-PI neat bcp.

IV. Discussion

IV.1. Phase Behavior as a Function of ϕ_{PS}. Figure 9 summarizes morphological investigation of the blends of SI dibcps α/*β*. With increasing amount of *β* which is rich in PS composition, the volume fraction of PS block in the blend, ϕ_{PS}, increases, and morphology of the blend changes from PS cylinder, lamella, and finally to PI cylinder. When the compositions are in the range $0.19 \leq \phi_{PS} \leq 0.36$, the blends form a hexagonally packed PS cylindrical microdomain. Increasing the composition in the range of $0.39 \leq \phi_{PS} \leq 0.48$ leads to an alternating lamellar structure. Further increasing ϕ_{PS} to 0.54, the blend exhibits a PI double gyroid in PS matrix. When the compositions reach the range $0.60 \leq \phi_{PS} \leq 0.71$, the blends possess PI cylindrical structure. The morphologies of neat SI dibcps have been identified very well. In the regime of a strong segregation limit, the following sequence of phases is observed in the composition range corresponding to our experiment as shown in Figure 9: $f_{PS} < 0.30$, PS cylinder; $0.30 \leq f_{PS} \leq 0.32$, PS gyroid; $0.32 < f_{PS} < 0.62$, alternating lamellae; $0.62 \leq f_{PS} \leq 0.67$, PI gyroid; $0.67 < f_{PS}$, PI cylinder,[29] where f_{PS} is volume fraction of PS block in neat SI dibcps.

Let us now compare the phase behavior of the blend with that of neat bcp. The comparison reveals that the blends have an extended composition range for cylinders but a narrowed composition range for lamella. A neat bcp having volume fraction of PS nearly 0.35, for example, has a small spontaneous curvature (see Figure 10a). When such a neat bcp is packed with its spontaneous curvature and without a significant change of conformation, a density dip around the center of PI microdomains is created or PI block chains must have stretched conformations as already discussed in conjunction with Figure 3c. Both cases need extra free energy cost and therefore are thermodynamically unstable. Thus, the packing constraint to

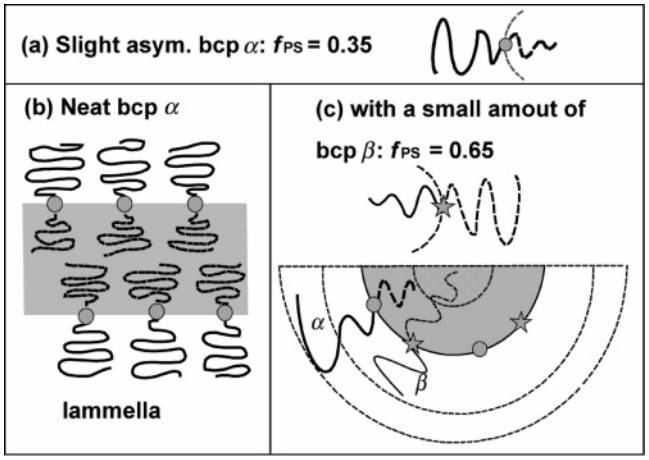

Figure 10. Schematic illustration of the cosurfactant effects narrowing the lamellar composition range: (a) a slightly asymmetric bcp α having a small spontaneous curvature, (b) packing constraint of neat, slightly asymmetric bcp α resulting in the formation of lamella, and (c) upon mixing of bcp β, the cosurfactant effect relaxes this packing effect to promote bcp α to take the spontaneous curvature.

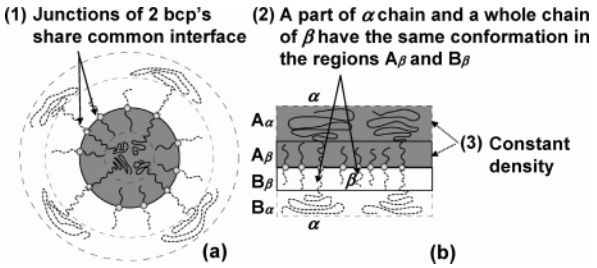

Figure 11. Schematic illustration of BZL model of blends of two bcps with different molecular weights and composition: (a) cylinder and (b) lamella.

satisfy the demand of incompressibility does not allow slightly asymmetric bcp to take the spontaneous curvature, resulting in lamellae formation, as shown in Figure 10b. However, when we mix a small fraction of bcp β, the long PI block chains of β fill the void space in the center of the PI domain without significantly changing the spontaneous curvature of α and without significantly imposing extra stretching of α and β chains (Figure 10c). Therefore, the cylinder is stabilized in the expanded composition range (0.3−0.36). The cosurfactant effects relax the packing constraint and stabilize the slightly asymmetric bcp to take the spontaneous curvature, which lead to the narrowed composition range for lamellae. The same story is applicable to the other side of composition range (PI cylinder), too. This is a manifestation of a cosurfactant effect for this blend system.

The observed expanded region of hexagonal cylinder phase at the expense of the lamellar phase is a generic phenomenon in mixtures of block copolymers. For example, Cooke and Shi[30] also found recently that the cylindrical phase is widened at the cost of the lamellar phase in their study of the phase behavior of polydisperse dibcps

IV.2. Quantitative Analysis with the BZL Theory. A. Brief Description of the BZL Theory. For more quantitative discussion of the effects, let us compare our results with BZL theory, the theory established by Birshtein and co-workers.[22−26] As schematically shown in Figure 11, the model assumes that a binary mixture of A−B bcps with different compositions which are miscible and form (a) a cylindrical microdomain or (b) a lamellar microdomain under strong segregation limit. The theory assumes that macrophase separation does not occur in the mixtures and that all their chemical junctions between A and B blocks share a common interface. The space of each microphase (i.e., A microdomain and B microdomain) is divided into two layers: the layer close to the interface (layer β) consists of short chains and a part of long chains which take the same conformation as the short chain, and the rest of long chains fill the other space (layer α) unoccupied by the short chains. The constant density is maintained everywhere in the domain space.

Here we shall not attempt to repeat the derivation as we did before,[31] but rather show only the resulting general expressions of the interface area per chain, σ_x, the free energy per chain, ΔF_x, and the characteristic domain size, R_x, corresponding to the thickness of B lamellae or the radius of B cylindrical domain. The details are available in the original papers.

$$\sigma_x = a^2 (N_{B,\beta})^{1/3} (PQ_x)^{1/3} \tag{2}$$

$$\Delta F_x = \frac{3}{2}\Phi (N_{B,\beta})^{1/3} (PQ_x)^{1/3} \tag{3}$$

$$R_x = i_x a (1 + \alpha_B n_S)(N_{B,\beta})^{2/3} (PQ_x)^{-1/3} \tag{4}$$

where x = C or L referring to cylinder or lamella, respectively, $i_C = 2$, $i_L = 1$, and a is the segmental length. The characteristic domain size, R_x, corresponding to the thickness of A lamellae or the radius of A cylindrical domain are obtained by exchanging the subscript of relevant parameters B and A in eqs 4−14 into the subscript A and B, respectively. n_S is the mole fraction of the short chain in the mixtures, and Φ is the surface free energy coefficient of the interface. α_j (j = A or B) is the relative difference between the degree of polymerization (DP) of j-th block chain in bcp α and β, given by eq 5:

$$\alpha_j = \frac{N_{j,\alpha} - N_{j,\beta}}{N_{j,\beta}} \tag{5}$$

where $N_{j,k}$ (j = A or B, k = α or β) is DP of of the jth block chain in bcp k.

$$P = \pi^2/(4\Phi p_B) \tag{6}$$

$$Q_C(n_S) = \frac{r^2}{2} G(\alpha_B, n_S) + \frac{p_B N_{A,\beta}}{p_A N_{B,\beta}} \frac{2(4 + 3h_{A\beta}/r)}{(2 + h_{A\beta}/r)^3} + \frac{p_B N_{A,\beta}}{p_A N_{B,\beta}} a_A n_S{}^3 \frac{2[4 + 3h_{A\alpha}/(r + h_{A\beta})]}{[2 + h_{A\alpha}/(r + h_{A\beta})]^3} \left(\frac{r}{r + h_{A\beta}}\right)^3 \tag{7}$$

$$Q_L(n_S) = 1 + \alpha_B n_S{}^3 + \frac{p_B N_{A,\beta}}{p_A N_{B,\beta}} (1 + \alpha_A n_S{}^3) \tag{8}$$

where p_j is the stiffness parameter of the jth polymer chain, given as $p_j = A_j/a$, and A_j is the Kuhn segment length. Parameters r, $h_{A\beta}$, and $h_{A\alpha}$ are given by eqs 9−11, respectively:

$$r = 2(1 + \alpha_B n_S) \tag{9}$$

$$\frac{h_{A\beta}}{r} = \sqrt{1 + \frac{N_{A,\beta}}{N_{B,\beta}}\left(\frac{1}{1 + \alpha_B n_S}\right)} - 1 \tag{10}$$

$$\frac{h_{A\alpha}}{r} = \sqrt{1 + \frac{N_{A,\beta}}{N_{B,\beta}}\left(\frac{1+\alpha_A n_S}{1+\alpha_B n_S}\right)} - \sqrt{1 + \frac{N_{A,\beta}}{N_{B,\beta}}\left(\frac{1}{1+\alpha_B n_S}\right)} \quad (11)$$

The function $G(\alpha_B, n_S)$ is rather complicated as described below:

$$\begin{aligned} G(\alpha_B, n_S) = (1+\alpha_B n_S)\{\sqrt{u^2 - l^2}[6u^2(1+\alpha_B) + \\ 0.5l^2 u(1 - 5\alpha_B - 10\alpha_B{}^2) - 0.5l^2(1+\alpha_B) - \\ u^3(6 - \alpha_B - 5\alpha_B{}^2)] + [-0.5l^4\alpha_B(1+5\alpha_B) + \\ 0.5l^2u^2(-10 + 3\alpha_B + 15\alpha_B{}^2) - 5u(u^2 - l^2)(1+\alpha_B) + \\ u^4(6 - \alpha_B - 5\alpha_B{}^2)]\} - 3l^2\alpha_B n_S \end{aligned} \quad (12)$$

where l and u are determined by the following equations:

$$\frac{n_S}{1+\alpha_B n_S} = \frac{\sqrt{1 - l^2(1-\alpha_B{}^2)} - \alpha_B}{1 - \alpha_B{}^2} - l^2 \ln \frac{l(1-\alpha_B)}{1 - \sqrt{1 - l^2(1-\alpha_B{}^2)}} \quad (13)$$

$$u = \frac{1 - \alpha_B\sqrt{1 - l^2(1-\alpha_B{}^2)}}{1 - \alpha_B{}^2} \quad (14)$$

Note that in this theory the monomer volume, υ, is assumed to be equal for both block chains for the simplicity and characterized by the segment length of a, as $\upsilon = a^3$. Taking into account the asymmetry in segmental volume, for the degree of polymerization, we used the modified values instead of the original values, $\overline{N_{j,k}}$ (j = PS or PI and $k = \alpha$ or β), which is given by

$$\overline{N_{j,k}} = (\upsilon_j/\upsilon_0)N_{j,k} \quad (15)$$

where $\upsilon_0 = (\upsilon_{PS}\upsilon_{PI})^{1/2}$, and we used the values of υ_{PS} and υ_{PI} as 107.2 and 81.9 cm^3/mol, respectively. We used the value of $\Phi = 0.3$ (in kT units with k and T being the Boltzmann constant and absolute temperature, respectively) for the sake of convenience. All these parameters can be found experimentally, so that there are no adjustable parameters. It should be noted that for neat bcps the strong segregation limit (SSL) is only available in the case when $\chi N \gg 10$, which is a rough limit for SSL behavior. Here χ and N are the Flory−Huggins segmental interaction parameter and DP of bcp, respectively. There are many studies on the estimation of χ parameter between PS and PI based on PS-*b*-PI copolymers with the relation as $\chi = A_\chi + B_\chi/T$.[32] Here A_χ and B_χ are constants. At our experimental temperature, 403 K, the value of χ is in the range 0.07−0.12. Therefore, we can estimate the values of χN for the two bcps in the range 28.4−81.4, indicating the system is in intermediate segregation regime. From SSL, the interfacial tension can be calculated by the relations $\Phi = p(\chi/6)^{1/2}$, where p is the stiffness parameter of the polymer chain. For PS-*b*-PI, we can estimate the values of Φ is in the range 0.13−0.17, which is slightly larger than that we used.

B. Comparison between Experimental and Theoretical Results. Figure 12 compares the experimental and theoretical results on interdomain distance and domain size as a function of total volume fraction of PS. The experimental data are shown by the symbol marks, and theoretical data are shown by solid curves. The curves on the left side of the vertical line (a) and (unfilled and filled) circles are for PS cylinder, the curves in between the lines (a) and (b) and symbols are for lamella, and the curves on the right hand of the line (b) and (unfilled and filled) triangles are for PI cylinder. Overall agreements are very good. More precisely, the two results satisfactorily agree in terms of absolute value of the domain size and distance and the composition where OOT occurs as well as the gap in the value of interdomain distance at OOT point. We would like to highlight that that the interdomain distance of the blend is much larger than that of the corresponding neat bcp. This is also an important cosurfactant effect. A good agreement was also obtained in the terms of domain sizes (radius of PS cylinder, PS lamellar thickness, PI lamellar thickness, and radius of PI cylinders).

It is interesting to note that at OOT point the radius of the cylinder becomes equal to the thickness of the lamella. At OOT point, it is easy to obtain the relations between the radius of the jth cylinder (R_j) and the thickness of the jth lamellae (L_j) as

$$\sigma_L L_j/2 = n_\alpha N_{j\alpha} a^3 + (1 - n_\alpha)N_{j\beta}a^3 = \sigma_C R_j/2 \quad (16)$$

where j = PS or PI and n_α is the mole fraction of block copolymer α at OOT point. The interface area per chain does not change at OOT point as shown in Figure 13, which gives rise to $\sigma_L = \sigma_C$ and hence $L_j = R_j$ at OOT point.

On the basis of the condition that the radius of cylinder is equal to the thickness of a lamella at OOT point, we have

$$D_C/D_L = (2\pi\phi_{PS,OOT}/\sqrt{3})^{1/2} \quad (17)$$

where D_C and D_L are the interdomain distance of cylindrical and lamellar microdomains, respectively, and $\phi_{PS,OOT}$ is the volume fraction of PS block chain. For example, at the transition point of PS lamella to PS cylinder, the theoretical value of $\phi_{PS,OOT}$ is 0.33 as shown in Figure 12, and we have $D_C/D_L = 1.09$. This indicates that there is a gap between the domain distance of cylindrical and lamellar microdomains at OOT point, which is also consistent with the experimental observation.

C. Comparison of Theoretical Phase Behaviors between Blends of BCPs and Neat BCPs. In Figure 14 we compare theoretical results between neat bcps and blends of PI-rich and PS-rich bcps having the same molecular weight (5×10^4) and different volume fractions of PS block (0.2 and 0.8), as shown in Table 3. Theoretical interdomain distances and domain sizes for the blends are shown by solid lines, while those for neat bcps are shown by broken lines. We find the following cosurfactant effects for the blends: First, the composition range for cylinders expands but that for lamella narrows; second, the interdomain distance expands, and the gap of the distance at OOT correspondingly expands. The cosurfactant effect also expands the domain size.

IV.3. Remarks on Cosurfactant Effects for Double-Gyroid Morphology. We anticipated the blending of the two bcps having the complementary compositions may expand the composition range for double-gyroid morphology. This is simply because a curvature distribution inherent in the gyroid may be stabilized by localization of bcps α and β having a different composition in relatively large and small cross-sectional areas of the network, as schematically shown in Figure 15. However, our experimental results do not tend to support this expectation. We found that the cosurfactant effect does hardly change the composition range of double gyroid. The SAXS and TEM studies for the blends exhibited the hex cylinder of PS up to the volume fraction of PS equal to 0.36 and lamellar morphology for the volume fraction of PS equal to or larger than 0.39 (see Figures 9 and 12). Therefore, if there are gyroids in between

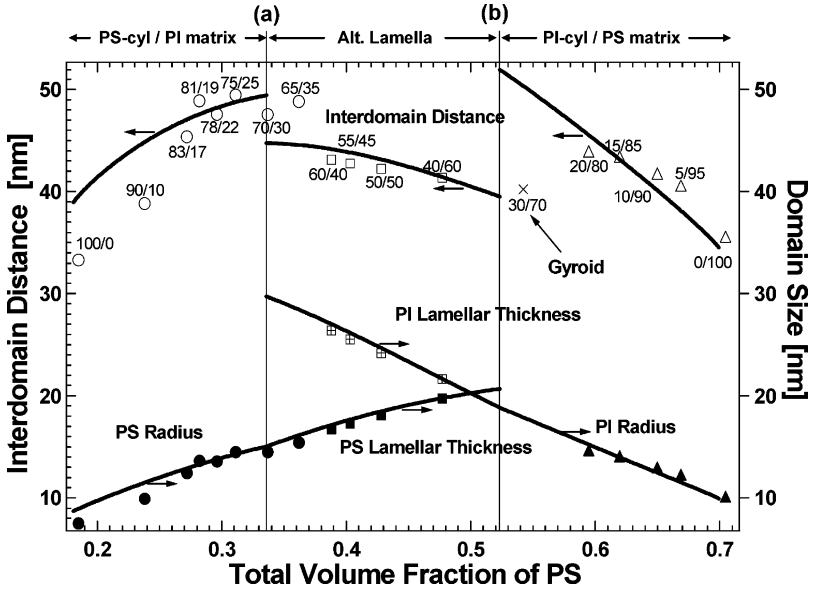

Figure 12. Comparison of the experimental and theoretical results on interdomain distance and domain size as a function of total volume fraction of PS. The experimental data for interdomain distance are shown by the symbol marks (unfilled circles, squares, and triangles for PS cylinder, alternating lamella, and PI cylinder, respectively) and those for domain size by symbol marks (filled circles, squares, and triangles for PS cylinder, alternating lamella, and PI cylinder, respectively), while theoretical data are shown by solid curves for both interdomain distance and domain size (PS radius, PI and PS lamellar thickness, and PI radius). The vertical lines (a) and (b) are theoretical boundaries among PS cylinder in PI matrix, alternating lamella, and PI cylinder in PS matrix.

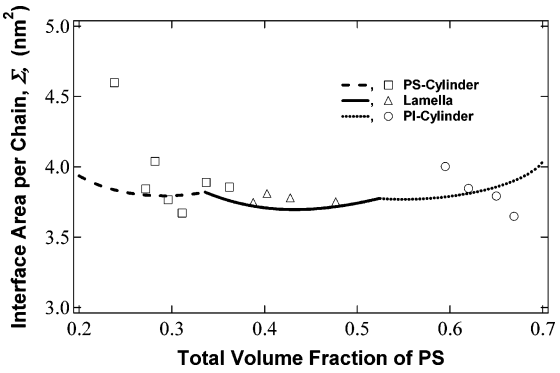

Figure 13. Comparison of the experimental and theoretical results on interface area per chain as a function of total volume fraction of PS. The experimental data are shown by the symbol marks (unfilled squares, triangles, and circles for PS cylinder, alternating lamella, and PI cylinder, respectively), while theoretical data are shown by broken, solid, and dotted curves, respectively.

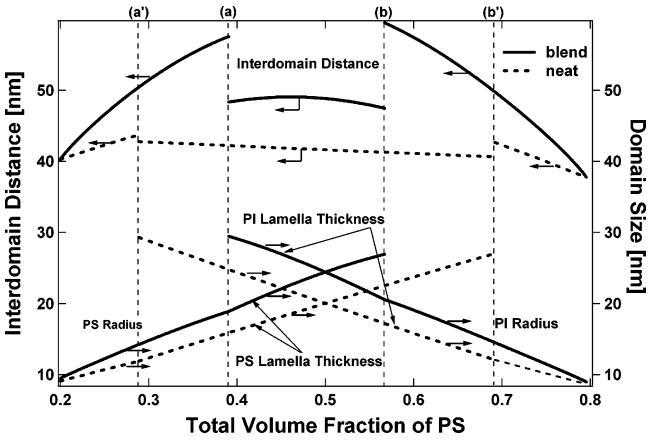

Figure 14. Comparison between the theoretical interdomain distances and domain sizes of a neat bcp (broken lines) and a blend of PI-rich and PS-rich bcps (solid lines) having the same molecular weight but different volume fractions of PS block. (a) and (b) are boundarys among PS cylinder in PI matrix and alternating lamellae and PI cylinder in PS matrix for the blend of the bcps, while (a′) and (b′) are those for neat bcp.

these compositions, the composition range is only 0.03 at a maximum. This composition range is almost identical to that of neat bcp (0.02), although the absolute value of ϕ_{PS} for the gyroid is shifted toward a large value due to the cosurfactant effect. It seem that the localized distribution of bcp chains α and β does not appear to offer a plausible model.

Our result appears to lead us to look at the cosurfactant effect from a different view point as follows. The gyroid phase may be considered to exist as a consequence of a compromise between the constant-curvature structure and the constant-thickness structure: the gyroid structure itself is neither a constant-curvature nor a constant-thickness structure. The cosurfactant effect favors constant-curvature structures and thereby may be negligible on the gyroid phase.

We observed the PI gyroid for the mixture having $\phi_{PS} = 0.54$. Except this composition, a relatively large composition range between lamellae ($\phi_{PS} = 0.48$) and PI cylinder ($\phi_{PS} = 0.60$) was left unexplored. A more precise exploration of morphologies vs composition is needed in this composition range as a future work before making a definite conclusion on the cosurfactant effect on gyroid morphology. It may be interesting to extend the studies of cosurfactant effects to binary mixtures of the gyroid-forming bcps having a complementary composition and almost the same molecular weights.

IV.4. Perspectives. The cosurfactant effects investigated in this work revealed an enlarged composition range for cylinders and tend to decouple composition of bcps and morphology. This is because for the neat bcp, hex cylinder for PS-*b*-PI copolymer exists in the composition range between 0.2 and 0.3, so that the morphology is closely coupled with the composition. However, the cosurfactant effects can vary the composition for hex cylinders. It may be possible to obtain hex cylinders having an extremely large volume fraction of cylinder.

On the basis of the BZL theory, we can predict that the PS cylinder is more stable than lamella for the cylinder volume fraction up to 0.64, for a special case when the ratio of molecular weights of the two bcps $r = 10$, the long bcp α has the PS

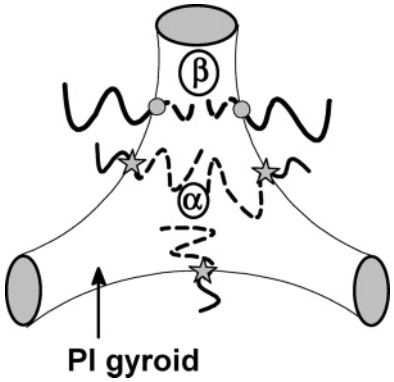

Figure 15. Schematic illustration of PI gyroid in PS matrix with the localization of bcps α rich in PI and bcps β rich in PS at the interface to fit a curvature distribution inherent in double gyroid.

Table 3. Characteristics of Diblock Copolymer Used in Theoretical Calculation

code	$M_n \times 10^{-4}$	f_{PS}
PI-rich	5.0	0.2
PS-rich	5.0	0.8

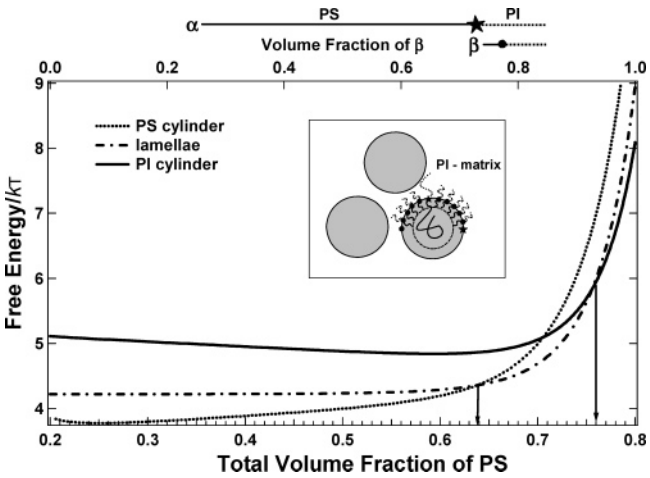

Figure 16. Prediction of hex cylinders having an extremely large volume fraction based on BZL theory on the basis of free energies of PS cylinder (dotted line), lamellae (dash-dotted line), and PI cylinder (solid line).

volume fraction of 0.8, and the short bcp β has the PS volume fraction of 0.2. In Figure 16 we plot the calculated value of free energies as a function of ϕ_{PS} and the volume fraction of short bcp β (shown on the upper abscissa) for a mixture of special pair of bcp α and β having different compositions ($f_{PS,\alpha} = 0.8$ and $f_{PS,\beta} = 0.2$) and molecular weights ($M_{n\alpha} = 100\,000$ and $M_{n\beta} = 10\,000$). The figure shows that the free energy of PS cylinder is lower than that of PI cylinder and lamellar even when the total fraction of PS block is as large as 0.64. In the inset to Figure 16 we present a schematic illustration of the very unique cylinder. In this case, the number of the short bcps β is much more than that of the long bcps α, although the short bcps β do not remarkably change the total volume fraction of PS due to the low molecular weight. However, those short chains locate the domain boundary interfaces, which may have a large effect on the interfacial energy, and therefore give rise to the stability of the special morphology. We should note that there is a possibility that the two bcp α and β undergo macrophase separation, though the theory does not account for the macrophase separation. Even in the case when the macrophase separation occurs, we can suppress the macrophase separation under such nonequilibrium conditions that the microphase separation occurs prior to the macrophase separation, which is followed by vitrification due to formation of glassy PS domains.

V. Conclusion

In this work we studied the blends of bcps which form PS cylinders in PI matrix and PI cylinders in PS matrix. Transmission electron microscopy and small-angle X-ray scattering were used to characterize the phase behavior and domain spacing and size of the domains. The results of all 16 blend specimens investigated show a single microdomain morphology which depends on blend compositions, implying that the two bcps are miscible at the molecular level and seemingly sharing the common microdomain interfaces, because of a high segregation condition employed in this work. First, we found an expanding composition range for hexagonally packed cylindrical morphology and a narrowed composition range for lamella relative to the behavior of neat SI bcps. The result indicates that the effects help bcp to take a spontaneous curvature. Second, it was found that the effects enlarged the domain size and spacing relative to corresponding neat bcps. This is also an important cosurfactant effect. Those results were compared with the BZL theory, which is proposed to predict strongly segregated binary bcp mixtures by Birshtein and co-workers. We found good agreements between experimental and theoretical results in terms of (i) domain size, (ii) interdomain distance, and (iii) the blending compositions where morphological transitions occur.

References and Notes

(1) (a) Hashimoto, T. In *Thermoplastic Elastomers, A Comprehensive Review*; Legge, N. R., Holden, G., Schroeder, H. E., Eds.; Hanser: Munich, 1996. (b) Hasegawa, H.; Hashimoto, T. In *Comprehensive Polymer Science, Second Supplement*; Aggarwal, S. L., Russo, S., Vol. Eds.; Pergamon: New York, 1996.
(2) Hamley, I. W. *The Physics of Block Copolymers*; Oxford University Press: Oxford, 1998.
(3) (a) Hashimoto, T.; Yamauchi, K.; Yamaguchi, D.; Hasegawa, H. *Macromol. Symp.* **2003**, *201*, 65. (b) Hashimoto, T.; Yamaguchi, D.; Court, F. *Macromol. Symp.* **2003**, *195*, 191.
(4) (a) Helfand, E. *J. Chem. Phys.* **1975**, *62*, 999. (b) Helfand, E. *Macromolecules* **1975**, *8*, 552.
(5) Meier, D. J. *J. Polym. Sci., Part C* **1969**, *26*, 81.
(6) (a) Hashimoto, T.; Yamasaki, K.; Koizumi, S.; Hasegawa, H. *Macromolecules* **1993**, *26*, 2895. (b) Hashimoto, T.; Koizumi, S.; Hasegawa, H. *Macromolecules* **1994**, *27*, 1562. (c) Koizumi, S.; Hasegawa, H.; Hashimoto, T. *Macromolecules* **1994**, *27*, 4371.
(7) (a) Yamaguchi, D.; Hashimoto, T. *Macromolecules* **2001**, *34*, 6495. (b) Yamaguchi, D.; Hashimoto, T. *Macromolecules* **2001**, *34*, 6506.
(8) (a) Court, F.; Hashimoto, T. *Macromolecules* **2001**, *34*, 2536. (b) Court, F.; Hashimoto, T. *Macromolecules* **2002**, *35*, 2566. (c) Court, F.; Yamaguchi, D.; Hashimoto, T. *Macromolecules* **2006**, *39*, 2596.
(9) Hadziioannou, G.; Skoulios, A. *Macromolecules* **1982**, *15*, 267.
(10) Spontak, R. J. *Macromolecules* **1994**, *27*, 6363.
(11) Spontak, R. J.; Fung, J. C.; Braunfeld, M. B.; Sedat, J. W.; Agard, D. A.; Kane, L.; Smith, S. D.; Satkowski, M. M.; Ashraf, A.; Hajduk, D. A.; Gruner, S. M. *Macromolecules* **1996**, *29*, 4494.
(12) Lin, E. K.; Gast, A. P.; Shi, A.-C.; Noolandi, J.; Smith, S. D. *Macromolecules* **1996**, *29*, 5920.
(13) Kane, L.; Satkowski, M. M.; Smith, S. D.; Spontak, R. J. *Macromolecules* **1996**, *29*, 8862.
(14) Sakurai, S.; Umeda, H.; Yoshida, A.; Nomura, S. *Macromolecules* **1997**, *30*, 7614.
(15) Sakurai, S.; Irie, H.; Umeda, H.; Nomura, S.; Lee, H. H.; Kim, J. K. *Macromolecules* **1998**, *31*, 336.
(16) Zhao, J.; Majumdar, B.; Schulz, M. F.; Bates, F. S.; Almdal, K.; Mortensen, K.; Hajduk, D. A.; Gruner, S. M. *Macromolecules* **1996**, *29*, 1204.
(17) Vilesov, A. D.; Floudas, G.; Pakula, T.; Melenevskaya, E. Y.; Birshtein, T. M.; Lyatskaya, Y. V. *Maromol. Chem. Phys.* **1994**, *195*, 3217.
(18) Shi, A.-C.; Noolandi, J. *Macromolecules* **1994**, *27*, 2936.
(19) Shi, A.-C.; Noolandi, J. *Macromolecules* **1995**, *28*, 3103.
(20) Matsen, M. W. *J. Chem. Phys.* **1995**, *103*, 3268.
(21) Matsen, M. W.; Bates, F. S. *Macromolecules* **1995**, *28*, 7298.
(22) Birshtein, T. M.; Lyatskaya, Y. V.; Zhulina, E. B. *Polymer* **1990**, *31*, 2185.

(23) Zhulina, E. B.; Birshtein, T. M. *Polymer* **1991**, *32*, 1299.
(24) Zhulina, E. B.; Lyatskaya, Y. V.; Birshtein, T. M. *Polymer* **1992**, *33*, 332.
(25) Lyatskaya, J. V.; Zhulina, E. B.; Birshtein, T. M. *Polymer* **1992**, *33*, 343.
(26) Birshtein, T. M.; Lyatskaya, Y. V.; Zhulina, E. B. *Polymer* **1992**, *33*, 2750.
(27) Hashimoto, T. *Macromolecules* **1982**, *15*, 1548.
(28) Hashimoto, T.; Kawamura, T.; Harada, M.; Tanaka, H. *Macromolecules* **1994**, *27*, 3063.
(29) Khandpur, A. K.; Foerster, S.; Bates, F. S.; Hamley, I. W.; Ryan, A. J.; Bras, W.; K.; Almdal, K.; Mortensen, K. *Macromolecules* **1995,** *28*, 8796.
(30) Cooke, D. M.; Shi, A.-C. *Macromolecules* **2006**, *39*, 6661.
(31) Yamaguchi, D.; Shiratake, S.; Hashimoto, T. *Macromolecules* **2000**, *33*, 8258.
(32) (a) Mori, K.; Okawara, A.; Hashimoto, T. *J. Chem. Phys.* **1996**, *104*, 7765. (b) Mori, K.; Hasegawa, H.; Hashimoto, T. *Polymer* **2001**, *42*, 3009.

MA070297M